baked at 300°C overnight) for varied amounts of time to the atmosphere of different working areas. Exposures of the test materials for short times (30 min or less) to the lab atmosphere and to a nitrogen-flushed glove box for sample preparation only gave rise to chemical background about a factor of 2 larger than the electronic noise. However, laboratory air was found to cover surfaces slowly (within many hours) with contaminants, some of which are believed to be PAHs originating from oil vapors or car exhaust entering the lab through the ventilation system.
20. Samples were from the meteorite collection at Arizona State University.
21. Crystalbond 509, Armeco Products, Inc., Ossining, NY.
22. Small glass balls dipped into a solution of coronene served as blanks for the chondrule machining. No coronene signal was detected after the glass balls were ground by the same method as described above and their interiors were analyzed; other contamination peaks were also negligible. These data indicate that material was not transferred from the outside by the grinding process. The thermoplastic polymer used for specimen mounting gave no background interferences.
23. Obtained from ChemService, West Chester, PA.
24. Benzene-methanol extractions of interior samples of Allende only gave about 0.002 ppm of aromatic hydrocarbons (*9*). This low concentration was speculated to result from organic material being trapped in the meteorite matrix (*7, 10*). In pyrolysis studies, up to 70 ppm of total organics were released (7), and aromatic compounds accounted for more than 75% of the total (*10*). One of the few PAHs reported is naphthalene, which had concentrations between 0.055 ppm (*10*) and 2 ppm (7).
25. C. C. A. H. Van der Stap, D. Heymann, R. D. Vis, H. Verheul, *J. Geophys. Res.* **91**, D373 (1986).
26. Some chondrules were mechanically split rather than ground, and in these too the signal was only at or below the chemical background level. These data support the contention that organics were not removed during the grinding process.
27. R. C. Weast, Ed., *CRC Handbook of Chemistry and Physics* (CRC Press, Boca Raton, ed. 68, 1987).
28. We thank K. Marti who provided us with some cleaned chondrules, C. B. Moore for samples, and B. C. Hintzman for assistance in computer interfacing this experiment. J.M.P. is grateful to the Swiss National Science Foundation for a postdoctoral fellowship. This work was supported by the National Science Foundation (NSF) Materials Research Laboratory program (grant NSF DMR 87-21735) through the Center for Materials Research at Stanford University (to R.N.Z.) and by National Aeronautics and Space Administration grant NAG9-59 (to P.R.B.).

6 June 1989; accepted 20 September 1989

Covariance Mapping: A Correlation Method Applied to Multiphoton Multiple Ionization

L. J. FRASINSKI, K. CODLING, P. A. HATHERLY

In some cases there are hidden correlations in a highly fluctuating signal, but these are lost in a conventional averaging procedure. Covariance mapping allows these correlations to be revealed unambiguously. As an example of the applicability of this technique, the dynamics of fragmentation of molecules ionized by an intense picosecond laser are analyzed.

IN AN INTERESTING APPLICATION OF the covariance approach, Hanbury Brown and Twiss used intensity interferometry to determine the angular diameter of stars (*1*). In their experiment the covariance between the signals from two independent telescopes was obtained as a function of telescope separation. We describe here an experiment in which the covariance concept is used to analyze the fragmentation pattern of molecules after multiple ionization by an intense subpicosecond laser (*2, 3*). In this experiment, the covariance is displayed in the form of a two- or three-dimensional map of competing fragmentation channels with axes given by ion time of flight (TOF).

When a molecule is rapidly ionized by the laser, a Coulomb explosion produces ion fragments with considerable kinetic energy and the fragment momentum vectors carry structural information about the parent molecule. To this extent such experiments are similar to those in which molecular ions are stripped of electrons by beam-foil techniques and in which TOF mass spectrometry is combined with an area detector to allow the stereochemical structure of the molecular ion to be inferred (*4*).

At each laser pulse only a few tens of ions are recorded, and this results in large pulse-to-pulse variations in the TOF spectra. These large variations can be overcome by averaging over many laser pulses. Even so, the analysis of the resulting TOF spectrum is often quite difficult because the fragment ion peaks of differing masses, charge states, and kinetic energies can overlap substantially. More importantly, the one-dimensional TOF spectrum suffers from two specific shortcomings. The first is that it is impossible to differentiate, for example, the process $[CO^{2+}] \rightarrow C^+ + O^+$ from the processes $[CO^+] \rightarrow C^+ + O$ and $[CO^+] \rightarrow C + O^+$, where undetected neutral particles are produced (brackets denote a transient molecular ion). Moreover, it is difficult to separate the process $[CO^{2+}] \rightarrow C^+ + O^+$ from the process $[CO^{3+}] \rightarrow C^{2+} + O^+$ if the O^+ ions have identical kinetic energies. [The problems associated with homonuclear molecules such as N_2 are even more severe (*3*).]

Covariance mapping allows the different fragmentation channels involving charged fragments to be identified conclusively. Consider a particular fragmentation channel of CO, namely, $CO \rightarrow [CO^{3+}] \rightarrow C^{2+} + O^+$, depicted in Fig. 1. Let us suppose that for a given laser pulse an O^+ fragment is detected. If it results from the above process, there is an enhanced probability of detecting a C^{2+} fragment. This probability is less than 100%, reflecting the detector efficiency. (The TOF system is designed to provide almost 100% collection efficiency.) When one calculates, over many laser pulses, the covariance between the two TOF points at which the fragments were detected, one

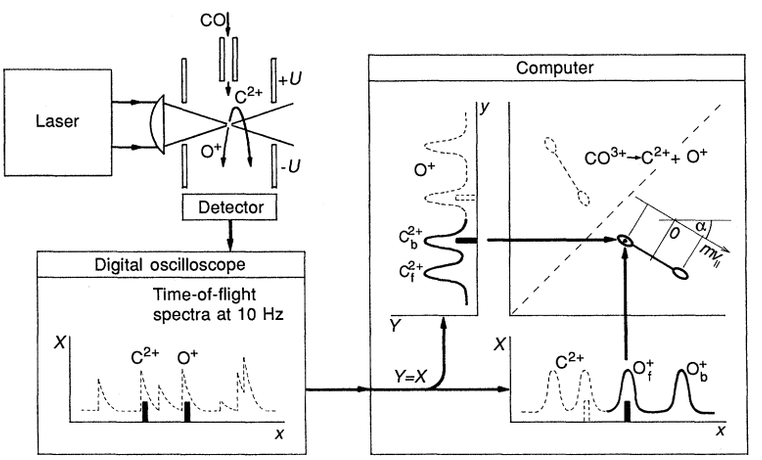

Fig. 1. The covariance mapping principle illustrated for a particular ionization and fragmentation channel of carbon monoxide, CO. One can identify the molecular parent ion by correlating the atomic daughter ions. The subscripts f and b denote forward and backward fragment ejection as seen by the detector.

J. J. Thomson Physical Laboratory, University of Reading, Whiteknights, Post Office Box 220, Reading RG6 2AF, United Kingdom.

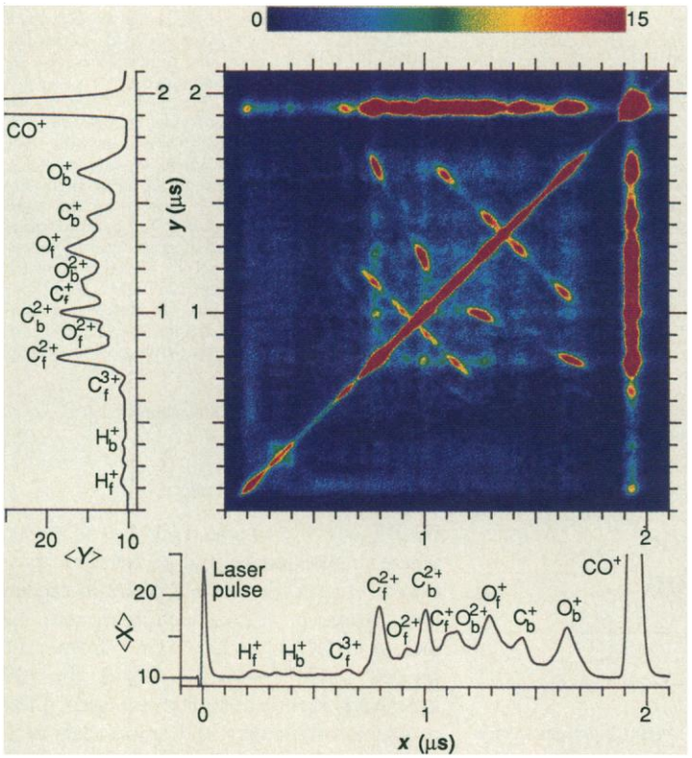

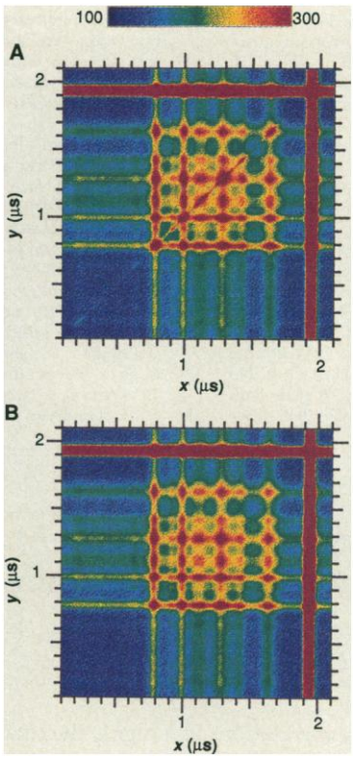

Fig. 2 (left). A covariance map showing the Coulomb explosion of CO induced by an intense laser field. X and Y are the signals from the detector in arbitrary units and x and y are the ion TOFs. The map was built up from $N = 26{,}000$ laser pulses with $U = 50$ V applied across the drift tube. [The structure associated with the CO^+ peak is an excess of uncorrelated product caused by fluctuations in the laser intensity. The unusual feature at low TOF is associated with protons from hydrocarbon impurities.] **Fig. 3 (right).** (**A**) The correlated product $\langle XY \rangle$ and (**B**) the uncorrelated product $\langle X \rangle \langle Y \rangle$. Their difference is the covariance map shown in Fig. 2. Notice the larger range of the color scale.

finds a positive value. Because one cannot know in advance which points in the TOF spectrum are correlated in such a fashion, one must calculate the covariance for each pair of TOF points and present it in the form of a two-dimensional map (Fig. 2).

The TOF spectrum from a single laser pulse, i, can be regarded as a sample function $X_i(x)$ of a random process (*5*), where the detector response, X, reflects the fluctuating number of ions at time x. In general, x can be a continuous variable but in the present experiment a digital oscilloscope is used to sample the TOF spectrum $X_i(x)$ at a number of discrete points x (typically 200). Therefore, $X_i(x)$ can be regarded as a 200-element vector indexed by x. Let us use a second label $Y_i(y)$ for the same vector $X_i(x)$ in order to have an unambiguous notation for their tensor product required to calculate the covariance matrix between each pair of TOF points x and y:

$$C(x,y) = \langle (X - \langle X \rangle)(Y - \langle Y \rangle) \rangle = \langle XY \rangle - \langle X \rangle \langle Y \rangle = \langle X(x)Y(y) \rangle - \langle X(x) \rangle \langle Y(y) \rangle = \frac{1}{N} \sum_{i=1}^{N} X_i(x)Y_i(y) - \left[\frac{1}{N} \sum_{i=1}^{N} X_i(x) \right] \left[\frac{1}{N} \sum_{i=1}^{N} Y_i(y) \right] \quad (1)$$

where the mean values $\langle\ \rangle$ are taken over N laser pulses (typically 20,000). The covariance map (Fig. 2) is the small difference between two large correlated and uncorrelated products $\langle XY \rangle$ and $\langle X \rangle \langle Y \rangle$ shown in Fig. 3, A and B.

In this particular covariance experiment, $X_i(x)$ and $Y_i(y)$ are the same ion TOF spectrum, and Eq. 1 is known as the autovariance function (*5*). This need not be the case, however. For example, $Y_i(y)$ can be an electron TOF spectrum recorded at the same time by a second detector. One consequence of using a single detector and taking $Y_i = X_i$ is the mirror symmetry of the covariance map, since $C(x,y) = C(y,x)$. Another is the strong diagonal autocorrelation line, which occurs simply because an ion pulse present on spectrum X_i at TOF x is always present on Y_i at $y = x$. The intensity along the ridge of the autocorrelation line is the variance $\langle X^2 \rangle - \langle X \rangle^2$ of the TOF spectrum. The intensity across the line is related to the time autocorrelation function (*5*), which reflects the instrumental time response.

The conventional scatter diagram (*6*) is a special case of the covariance map and can be obtained if one makes three simplifications. (i) The average counting rate must be reduced to about one event per TOF spectrum; (ii) the spectrum values (X_i and Y_i) must be 1 or 0 (either an event occurs or it does not); and (iii) the division by N is not performed. In this case the $N\langle XY \rangle$ term is the number of coincidence events and $N\langle X \rangle \langle Y \rangle$ is negligibly small. An example of this technique is the triple coincidence method applied to the fragmentation of molecules ionized by synchrotron radiation (*7*).

In order to interpret the map quantitatively, we have performed a computer simulation of the process depicted in Fig. 1 for a single point on the map but off the autocorrelation line. In the focal spot of the laser, the number of parent ions created was assumed to have a Poisson distribution. The most important result of the simulation was that the covariance signal is linearly proportional to the number of parent ions. Therefore, the covariance map shows directly the relative abundance of the various parent ions and their fragmentation channels. One also finds that the signal-to-noise ratio for the map is independent of the number of parent ions. This means that the signal-to-noise ratio is not degraded at a high event rate, even when many ion pulses arrive at the same TOF, a somewhat surprising result.

In order to understand the shape of the features on the covariance map, it is necessary to describe the fragment trajectories in the TOF spectrometer. The geometry is such that the electric field of the laser light lies along the drift tube. A molecule is more easily ionized when its axis is along the electric field (*2*), and, because there is no time for molecular rotation, the Coulomb explosion ejects the fragments along the drift tube axis, either toward or away from the detector. The potential U (Fig. 1) applied to the drift tube forces all fragments toward the detector. For a given fragment

mass, m, and charge, q, TOF varies linearly with the initial momentum component along the drift tube axis, $mv_{||}$, provided that the initial kinetic energy is not too large. That is, the TOF

$$x = A\,(m/qU)^{1/2} + B\,mv_{||}/(qU) \qquad (2)$$

valid for $mv_{||}^2/2 \leq 0.1\,qU$, where A and B are instrumental constants. This results in two groups of fragment ions, "forward" ions that are ejected initially toward the detector ($mv_{||} < 0$) and "backward" ions that are ejected away ($mv_{||} > 0$).

It follows from Eq. 2 that in these experiments the covariance map is a momentum correlation diagram. In the case of a two-body fragmentation, momentum conservation requires the correlated structure to be in the form of a line. The two islands on each line reflect the forward-backward and backward-forward fragment correlation (Fig. 1). The line tilt angle, α, reflects the fragment charge ratio, and the intensity variation along the line gives the momentum distribution. The different ionization and fragmentation channels are represented by different pairs of islands on the covariance map (Fig. 2). We can now see that the broad O^+ peak in the $\langle X \rangle$ spectrum lying at 1.65 μs in Fig. 2 is in reality associated with three different channels on the map: $[CO^{2+}] \rightarrow C^+ + O^+$, $[CO^{3+}] \rightarrow C^{2+} + O^+$, and (weak) $[CO^{4+}] \rightarrow C^{3+} + O^+$.

Three-body processes will clearly add more structure to the covariance map. In the case of a linear molecule such as N_2O, the Coulomb explosion leaves the middle fragment, N_m, with a small kinetic energy (Fig. 4A). The outer fragments are ejected in almost opposite directions and produce tilted correlation lines similar to those in the diatomic case. The additional vertical and horizontal lines represent correlations of an outer fragment with the middle one. The nonuniform width and tilt of all lines reflect the residual momentum of the middle fragment.

In the case of a bent triatomic molecule such as SO_2, the middle fragment, S, carries significant momentum (Fig. 4B). The correlation lines are now much broader. They start to overlap one another, creating a single overall elliptical shape with six maxima. Indeed, one expects an ellipse to be seen on the map if the three fragment momenta are fixed relatively to each other but are free to rotate as a whole. The broad maxima tell us that the ionization is enhanced when the molecule is roughly aligned along the electric field of the light wave.

Correlations between three points on the TOF signal can be explicitly shown on a three-dimensional covariance map by a natural extension of Eq. 1:

$$C(x,y,z) = \langle (X - \langle X \rangle)(Y - \langle Y \rangle)(Z - \langle Z \rangle) \rangle$$

There is, of course, a price to pay for adding another dimension to the map. The covariance signal is reduced because the detection efficiency of the third ion is now involved. Only a fraction of the map volume can at present be observed in one experimental run because the computer can process only a limited number of data points. However, more sophisticated processing of multidimensional covariance maps would allow the study of polyatomic molecules with high momentum resolution. Specific cross sections through the map volume could be used to select the interesting fragmentation channels and thereby limit the number of points that need to be processed.

Covariance mapping should be recognized as a general technique. It can undoubtedly be applied to any TOF beam experiment where pulsed laser, electron, ion, or neutral particle beams are targeted on free molecules, clusters, or surfaces. It may have application to any repetitive signal with fluctuations reflecting some underlying correlated process. The signal can be a function of time, position, frequency, or other parameter of the measurement process. Moreover, such maps can be created with the use of signals from different detectors that are measuring different physical quantities.

Note added in proof: Huang *et al.* (*8*) use a related but more restricted approach to associate ions by TOF mass spectrometry. They present correlation coefficients for ions in tabular form.

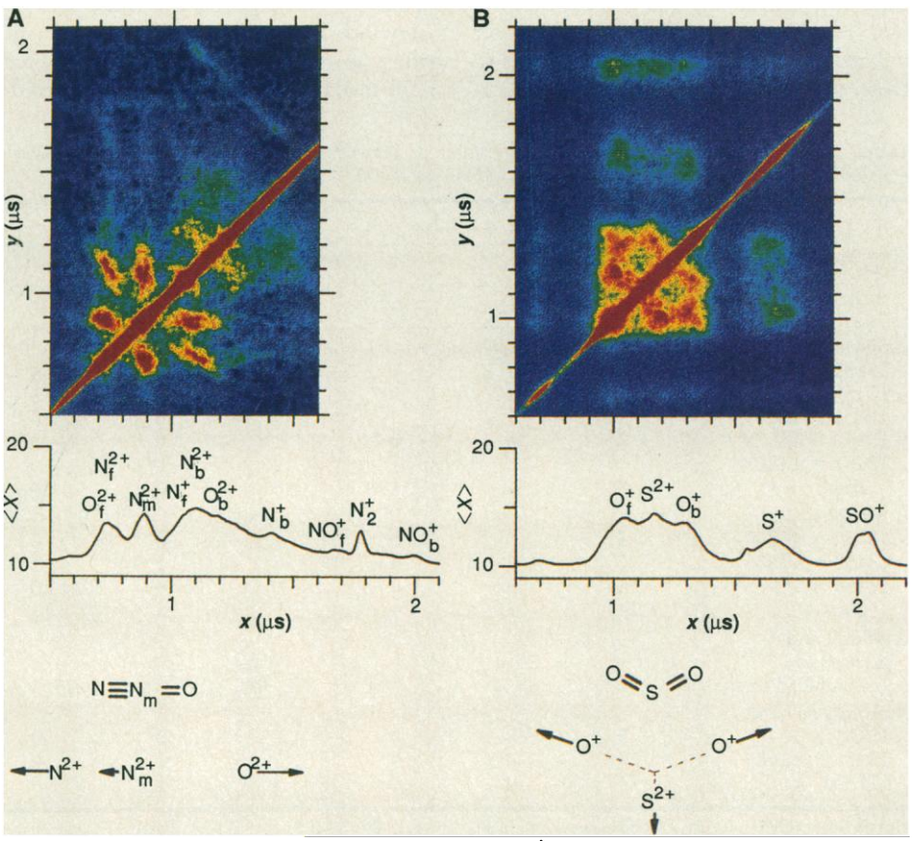

Fig. 4. The Coulomb explosion of (**A**) a linear molecule, N_2O, and (**B**) a bent triatomic molecule, SO_2. The fragmentation diagrams at the bottom describe the strong sextuple features on the covariance maps. The subscript m denotes the middle nitrogen atom. The weak line at 45° in the top right corner of map (A) corresponds to the $[N_2O^{2+}] \rightarrow N^+ + NO^+$ fragmentation channel. The laser polarization was parallel to the drift tube axis. The tube potential was U = 60 V for (A) and U = 80 V for (B).

REFERENCES AND NOTES

1. R. Hanbury Brown, *The Intensity Interferometer* (Taylor and Francis, London, 1974).
2. L. J. Frasinski *et al.*, *Phys. Rev. Lett.* **58**, 2424 (1987).
3. K. Boyer *et al.*, *Phys. Rev. A* **39**, 1186 (1989).
4. Z. Vager *et al.*, *Science* **244**, 426 (1989).
5. J. W. Goodman, *Statistical Optics* (Wiley, New York, 1985).
6. W. J. Krzanowski, *Principles of Multivariate Analysis* (Clarendon, Oxford, 1988).
7. L. J. Frasinski *et al.*, *J. Phys. B* **19**, L819 (1986).
8. L. Q. Huang, R. J. Conzemius, G. A. Junk, R. S. Houk, *Int. J. Mass Spectrom. Ion Processes* **90**, 85 (1989).

9. Financial support and the use of the Laser Support Facility were provided by the Science and Engineering Research Council of the United Kingdom. We are particularly indebted to W. T. Toner for helpful comments about the covariance mapping technique and to M. P. Millard for the machining of equipment.

16 May 1989; accepted 15 August 1989